

MASS TRANSPORT IN THE INTERNAL REFORMING HYDROCARBON ANODE

William R. Alcorn

Leesona Moos Laboratories
Great Neck, New York

INTRODUCTION

An alkaline-electrolyte fuel cell based on an internal-reforming anode offers advantages of heat economy, compactness, and controllability over an external-reforming cell. (8, 11) The operating principle is illustrated in Figure 1. Experimental work has been reported for methanol (2) and hydrocarbons. (1, 3) In the preferred temperature range, 400 - 500° F, the thermodynamics of methanol reforming are favorable, permitting high current densities. The conversion of saturated hydrocarbons into hydrogen, however, is severely restricted by thermodynamics.

During the present investigation we have studied catalyst decay, anode preparation, thermodynamic limitations, and the performance of an experimental anode with methane. This paper is concerned with the last topic, and specifically with an examination of the limitations on performance and changes that might be made to maximize performance. The present performance goal for a liquid hydrocarbon fuel such as octane is approximately 100 amps/ft² at 500° F, 200 mV anode polarization (a full cell voltage of about .90 V), and 70% fuel utilization.

ANALYTICAL TREATMENT OF ANODE CELL PROCESSES

Figure 2 illustrates the cell dimensions used in the discussion. For fixed pressure, temperature, and fuel/water ratio, fuel flow rate may be taken as proportional to average velocity times cross-sectional area:

$$Q_F \propto uat \quad (1)$$

Current density is based on membrane area:

$$I/A = I/aL \quad (2)$$

Fuel utilization is proportional to total current divided by fuel flow rate:

$$\eta_u \propto \frac{I}{Q_F} = \frac{(I/A) aL}{uat} = \frac{(I/A) L}{u t} \quad (3)$$

Data are reported in terms of the ideal hydrogen space velocity, which is volumetric flow of hydrogen (NTP) that would be produced by complete conversion of fuel, divided by cell volume. From equation (1) we note that:

$$S_v \propto \frac{uat}{aLt} = \frac{u}{L} \quad (4)$$

Utilization versus Current Density

As flow velocity is varied through an anode cell at fixed potential, the resulting current density will exhibit a maximum although it may occur at very low utilization. At very low flow rates, complete utilization is accomplished and current density is proportional to flow rate. At very high flow rates, the residence time is short and the average hydrogen concentration decreases towards zero, causing a decrease in I/A . These limits are shown in Figure 3 as a function of S_Y . Note that the proportional relation at low flow rate is an asymptote of slope + 1 on a log-log plot.

In determining the operating point to achieve a specified utilization and maximum I/A , two cases may be distinguished, depending on whether increasing flow rate has a beneficial effect on I/A through its effect on mass-transfer processes.

1. If there is no such effect, e. g., if transport is purely by molecular diffusion, then space velocity is set to give the desired utilization, and I/A is determined by reaction kinetics and utilization.
2. If I/A increases with flow rate over some range, e. g.,

$$I/A \propto u^n \quad (5)$$

where mass-transfer data suggest $0 < n < 0.5$ (see later), then from equation (3) at fixed bed thickness,

$$\eta_u \propto \frac{L}{u^{1-n}} \quad (6)$$

Thus, from equations (5) and (6) the design procedure would be to maximize I/A with respect to flow rate in a "short", one-pass cell and then increase the effective length of the anode to obtain the desired utilization. The average I/A will be lower than the maximum obtained in the short cell, but it should nevertheless be a maximum at the desired utilization.

There are various ways to increase effective flow length which are used in analogous situations: series gas flow through connected anode cells, partial recycle of gas, and internal baffling of the flow path. The three differ mainly in the way pumping power is introduced and dissipated, and in their effect on system control and reliability.

In any case, one expects that the optimization of an internal-reforming cell should involve a tradeoff between cost of pumping and the enhanced mass (and heat) transfer obtainable with high-velocity flow. In fact, a "perfect catalyst" might be defined as one so active that this optimization is required.

High-Velocity Range

As shown on Figure 3, I/A is depressed at low flow rates because of the extraction of hydrogen. In other words, the maximum available (equilibrium) hydrogen partial pressure decreases as utilization increases. For instance, for a 2.7 H₂O/CH₄ mixture at 500° F, the equilibrium p_H is 29 mm Hg with no extraction, and 9.1 mm Hg with 70% extraction of ideal hydrogen.

In the high-velocity range where utilization is low, I/A depends on both mass-transfer and reaction rates. As a first approximation, we assume that I/A, or H₂ flux toward the membrane, is proportional to a mass-transfer coefficient and a maximum available hydrogen partial pressure,

$$I/A \propto k_m p_H \quad (7)$$

As flow rate is increased, k_m will increase because of increasing convective diffusion and p_H will decrease because of kinetic rate limitations.

For this analysis it is assumed that k_m obeys the conventional correlation for mass transfer between particles and a flowing fluid:⁽⁴⁾

$$k_m \propto u^n \quad (0 < n < .5) \quad (8)$$

This is shown in Figure 4. The point of transition is designated S_x; it occurs near a particle Reynolds number of 1. The curve in Figure 4 may be satisfactorily represented by the following equation:

$$\frac{k_m}{k_o} = 1 + \left(\frac{S_v}{S_x} \right)^{.5} \quad (9)$$

Reaction Kinetics and Open-Circuit Behavior

Lacking knowledge of the true kinetic relations, the generation of H₂ is simply represented here as a first-order rate process which decreases as equilibrium is approached:

$$\frac{\text{rate}}{\text{unit volume bed}} = \frac{k_r}{RT} (p_{eq} - p_H) \quad (\text{mols/hr-cm}^3) \quad (10)$$

With the assumptions of no extraction (open circuit), plug flow, and zero H₂ concentration at the entrance, a differential mass balance on H₂ gives the following relation between local H₂ pressure and distance through the cell:

$$\frac{p_H}{p_{eq}} = 1 - \exp \left(- \frac{k_r}{S_v} \frac{x}{L} \right) \quad (11)$$

We wish to relate this H_2 gradient to the open-circuit voltage (OCV). Tests with known H_2/N_2 streams confirmed that the measured OCV corresponded closely to the theoretical value:

$$OCV = \frac{RT}{2F} \left(\ln \frac{760}{P_{eq}} - \ln \frac{P_H}{P_{eq}} \right) \quad (12)$$

In the presence of a pressure gradient, however, it is not physically obvious whether the observed OCV reflects an average partial pressure or an average potential with respect to anode length. In the first case the right-hand term becomes

$$\overline{\ln \left(P_H/P_{eq} \right)} = \ln \int_0^1 \left(P_H/P_{eq} \right) d(x/L) \quad (13)$$

and the integral is

$$\frac{\overline{P_H}}{P_{eq}} = 1 - \frac{\left[1 - \exp \left(-k_r/S_v \right) \right]}{k_r/S_v} \quad (14)$$

In the second case

$$\overline{\ln \left(P_H/P_{eq} \right)} = \int_0^1 \ln \left(P_H/P_{eq} \right) d(x/L) = \frac{S_v}{k_r} \sum_{n=1}^{\infty} \frac{\left[1 - \exp \left(-nk_r/S_v \right) \right]}{n^2} \quad (15)$$

Curves of OCV versus S_v for various k_r 's are presented for the two calculation methods in Figures 5a and 5b respectively.

Flow-Rate Effect on Current Density

In a cell at fixed anode potential the current density depends on both mass-transfer and reaction rates, which in turn depend on flow (convection) rate. A nondimensional equation expressing these relations has been developed, based on equations (7), (9) and (10). The result is that the current ratio I_R is a function of three ratios of characteristic rates:

$$I_R = \frac{(I/A)}{\left(\frac{k_o p_{eq}}{RT} \right)} = f \left(\frac{S_v}{k_r}, \frac{S_x}{k_r}, \frac{k_o/t}{k_r} \right) \quad (16)$$

where,

| | | |
|---------|----------|---|
| S_v | \equiv | convection rate |
| k_r | \equiv | reaction rate |
| k_o/t | \equiv | mass-transfer rate |
| S_x | \equiv | transition space velocity for mass-transfer correlation, equation (9) |

We have generated plots of I_R versus S_v/k_r for several values of the other two parameters. Representative curves are shown in Figure 6. Equation (16) applies directly to the high-flow region where p_{eq} is constant. It is also applicable to the low-flow region where extraction depresses the equilibrium H_2 concentration, if it is combined with an appropriate equation for p_{eq} as a function of flow rate. The following generalizations may be made from the results.

1. A significant maximum is obtained only when the transition in the mass-transfer relation occurs at a low velocity $(S_x/k_r \ll 1)$. Otherwise the current density decreases with flow velocity in approximately the same way as does \bar{p}_H (equation 14).
2. Whether or not a significant maximum occurs, the current density always begins to decrease rapidly in the range $.2 < S_v/k_r < 2$.
3. The relative mass-transfer coefficient has a major effect on the absolute value of I/A but it has little effect on the relation between I/A and flow rate.

EXPERIMENTAL

Three types of data from the anode cell are presented: OCV versus S_v , I/A versus S_v , and OCV versus time when flow was stopped. Flow-visualization tests are also discussed.

Apparatus

The anode assembly consisted of a .001 inch 75 Pd/25 Ag activated membrane, 1.5 x 2.5 inches, backed up by a .187 or .125 inch thick bed of 20-mesh nickel catalyst (Girdler G60RS). Gas entered and left the cell through small ports along the 1.5 inch sides which in turn led to .25 inch tubes positioned at diagonally opposite corners of the holder. The feed was preheated H_2O/CH_4 in a mole ratio of 2.7/1. The anode was run as a half cell in 85% KOH at 500°F. The potential reference was 1 atm H_2 in a Pd-Ag tube in an etched Teflon Luggin capillary. Current density (no IR correction) was measured potentiostatically with an Anotrol controller, usually at an anode potential of 200 mV versus reference. Effluent was analyzed with a gas chromatograph. Performance was not significantly affected by 25% changes in the H_2O/CH_4 ratio, by pressurization of

the cell up to 20 inches H_2O , nor by vertical versus horizontal orientation of the anode in the electrolyte.

Open Circuit Voltage

Figures 5a and 5b show OCV data for three runs, including two bed thicknesses and both horizontal and vertical orientation of the anode. Fluctuations of OCV over several minutes are indicated by the height of the data points. According to the pressure-averaging method, k_r is about 3000 hours⁻¹; by the potential-averaging method it is about 15,000 hours⁻¹. The latter method fits the data better; it is mathematically correct if one accepts that the measured potential of a metallic electrode is the area average of point potentials and that a large potential gradient may be sustained in the plane of the electrode.

Current Density

Points from the same three runs along with data from previous work⁽³⁾ are shown in Figure 7. These current densities are the steady values after several minutes; initial currents were generally 1.6 to 2.0 times the final values. Although experimental problems limited the flow range that could be tested, it may be seen that I/A decreases at both low and high flow rates, corresponding qualitatively with the analytical curves in Figure 6.

A rough estimate of k_r can be made from equation (10) and the total H_2 generation rate, which is the sum of current flux plus H_2 in cell effluent. For $I/A = 80$ amps/ft² at $S_v = 3000$ hours⁻¹ in the .187 inch bed, we assume the average p_H in cell and effluent to be half of p_{eq} (29 mm Hg). Then H_2 rate as current is .039 mols/hr, and in the effluent .026 mols/hr, with the result that $k_r \cong 13,000$ hours⁻¹.

Transient Behavior

An alternative way to measure the anode rate processes is to observe the change in OCV with time when flow is stopped. This was done during the same three runs. Figure 8 shows that OCV approaches the equilibrium value for CH_4 and H_2O (about 75 mV at 500° F), but requires several minutes to do so.

Flow Distribution

Some room temperature flow-visualization tests were made on the anode cell with a transparent window in place of the membrane. The cell was packed with indicating Drierite, and water-saturated N_2 was passed through at experimental flow rates. A peaked color profile was seen to move through the bed, the main flow taking a diagonal path between holder inlet and exit in spite of the small-diameter gas ports which had been intended to distribute the flow.

DISCUSSION

The open-circuit data (Figure 5) show that the simple model is adequate to describe the relationship between flow rate and kinetics, and k_x is about 3000 or 15,000 hours⁻¹, depending on how OCV is related to the gas-side gradient of p_H . The higher or potential-averaged value is supported by a better fit of data to theoretical curves and by a separate calculation of k_x from observed current density. Current densities (Figure 7) are unacceptably low, but in a qualitative sense are consistent with the model developed. On the basis of these two types of data one might conclude that catalyst activity is the major barrier to higher performance. However, arguments based on the transient behavior of OCV (Figure 8) and supporting calculations indicate a major role for mass transfer. These are discussed below.

Maximum Attainable Rate

It is important first to estimate the current density that could be achieved under various ideal conditions. The first case of interest concerns the current that could be supported by the activated .001 inch membrane if it were exposed to a gas mixture in equilibrium. A curve of I/A versus p_H for 500° F and 200 mV polarization has been estimated from previous unpublished data. Combining this curve with equilibrium calculations for $H_2O/C = 2.7$, Table 1 shows the estimated maximum performance for methane and octane at both zero and 70% utilization. Experimentally, the best current densities shown in this and previous work are about 35 - 45% of the tabulated values.

Table 1. Maximum Attainable Performance With .001 Inch Pd-Ag Anode, 500° F, 200 mV Polarization

| Fuel | η_u (%) | Average p_H (mm Hg) | I/A (amps/ft ²) |
|----------------|--------------|--------------------------|----------------------------------|
| C ₁ | 0 | 29 | 330 |
| C ₁ | 70 | 14 | 210 |
| C ₈ | 0 | 17 | 240 |
| C ₈ | 70 | 12 | 190 |

Transient Behavior

Four processes may be postulated to account for the characteristic open-circuit equilibration time of several minutes (Figure 8).

1. reaction rate
2. orientation of the cell as it affects flow distribution

3. solution of H_2 in the Pd-Ag membrane
4. diffusion in the catalyst bed

The reaction kinetics may be checked by integrating equation (10). Then the time required for p_H to change from p_1 to p_2 is

$$\Delta t \text{ (min)} = \frac{60}{k_r} \ln \frac{p_{eq} - p_1}{p_{eq} - p_2} \quad (17)$$

Taking $k_r = 3000 \text{ hours}^{-1}$ from Figure 5a, $p_{eq} = 29 \text{ mm Hg}$, $p_1 = 5$, and $p_2 = 28$, $\Delta t = .064 \text{ min} = 3.8 \text{ seconds}$. Larger values of k_r give even shorter times. Since there is so great a discrepancy between this and the observed equilibration time, some kind of diffusion process must be involved.

The anode orientation was changed from horizontal (membrane facing up) to vertical in order to ensure catalyst being in contact with the membrane and to decrease flow channeling that would probably occur if a gas gap existed. No significant change in performance or equilibration time resulted from this change, and we conclude that neither blockage of the membrane nor the existence of a gas space next to the membrane could account for the long equilibration times.

On the basis of unpublished data⁽⁷⁾ and previous work,^(6, 10) we estimate the solubility of H_2 in the membrane to be about 0.7 cc (NTP) at $p_H = 5 \text{ mm Hg}$ and 1.5 cc (NTP) at $p_H = 28 \text{ mm Hg}$. In comparison, the gas space only contains about .16 cc of H_2 (NTP) at the higher pressure. Thus, during equilibration most of the H_2 produced is absorbed by the membrane. If the membrane is at all times in equilibrium with the gas, then by a calculation similar to equation (17) we estimate equilibration time (5 to 28 mm Hg) to be about 8 seconds. The current density supported by the membrane shows that the absorption rate is very rapid, so if the membrane solubility contributes to the long equilibration time it is because of slow diffusion of H_2 toward it.

Mass Transfer in Catalyst Bed

Three kinds of mass transfer may be important: pore diffusion in the catalyst particles, transport of reactants and products between bulk gas and catalyst, and transport of H_2 through the bed to the membrane. It may be shown that the first two processes are quite rapid relative to observed net reaction rates. For example, using standard correlations,⁽⁴⁾ we estimate the bulk mass-transfer coefficient (the second process) to be on the order of 100 times the first-order reaction rate coefficient in the same units.

The third process, although related to the second, occurs on a larger scale, i. e., it involves a concentration gradient across the thickness of the catalyst chamber. To a first approximation, we may define the H_2 flux in the x-direction (as current density) in terms of an effective diffusivity D_e :

$$l/A \propto \frac{D_e}{RT} \frac{d p_H}{d x} \quad (18)$$

It should be noted that the coefficient k_m , as used in the mathematical analysis, and D_e describe the same process although defined in different dimensional terms. D_e is used for convenience in estimating.

D_e may be estimated by two methods. First, it may be calculated from molecular diffusivity and modified to account for the porous bed structure by an empirical equation:⁽⁹⁾

$$D_e = \frac{\epsilon}{\tau} D \quad (19)$$

For a characteristic multicomponent mixture of H_2O , CH_4 , H_2 , and CO_2 at $500^\circ F$, D_{H_2} is about $2.1 \text{ cm}^2/\text{sec}$ and diffusivities of the other three gases range from $.45$ to $.75 \text{ cm}^2/\text{sec}$. Measured bed porosity $\epsilon = .42$ and tortuosity τ for an unconsolidated bed is generally 1.5 to 2.0 .⁽⁹⁾ Then D_e is about $0.5 \text{ cm}^2/\text{sec}$ for H_2 and 0.1 to 0.2 for the other gases.

Secondly, if turbulent (convective) diffusion is the dominant transport process normal to the membrane, D_e may be estimated from the Peclet number:

$$P_e = \frac{d u}{D_e} \quad (20)$$

Taking $d = .084 \text{ cm}$, the interstitial velocity $u = 22 \text{ cm/sec}$ (corresponding to $S_v = 3000 \text{ hours}^{-1}$ in the $.187 \text{ inch}$ cell), and the Peclet number to be 13.6 ,⁽⁴⁾ D_e is approximately $0.14 \text{ cm}^2/\text{sec}$. That it is about the same magnitude as the effective molecular diffusivity implies that both molecular and turbulent diffusion are important at this flow rate. Below a space velocity of about 1000 hours^{-1} molecular diffusion dominates the lateral transport process.

The values of D_e may now be used in estimating the transient equilibration time due to diffusion. We start with the solution of the equation for one-dimensional diffusion from a surface source,⁽⁵⁾ and focus on the relative partial pressures at the source and a fixed distance from it -- in this case half the cell width (1.9 cm). Letting f = the ratio of partial pressures at the fixed point to the source, the time elapsed between f_1 and f_2 is

$$\Delta t = \frac{(1.9)^2}{4 D_e} \left[\frac{1}{\ln f_1} - \frac{1}{\ln f_2} \right] \quad (21)$$

Assuming that the initial p_H at the edge is 50% that at the center ($f_1 = .5$), equilibration times are shown in Table 2 for two final partial-pressure ratios, for H_2 ($D_e = .5$) and for the average of the other gases ($D_e = .15$).

Table 2. Transient Diffusion Times (Equation 21)

| | Δt (min) | |
|-------------|---------------------------|-----|
| | D_e (cm^2/sec) = .5 | .15 |
| $f_2 = .95$ | 0.5 | 1.6 |
| $f_2 = .99$ | 2.8 | 9.3 |

The calculation probably underestimates diffusion time because no account is taken of the solubility of H_2 in the membrane (see earlier). We conclude that diffusion in the catalyst bed is a reasonable explanation for the observed equilibration times of several minutes. It is not possible to say whether the main diffusion process is parallel to the membrane (e. g., if there are "stagnant" corners which must come to equilibrium) or normal to the membrane in the process of absorption of H_2 into the Pd-Ag.

To estimate the current density with an "ideal" catalyst and real diffusion resistance, we assume the partial-pressure gradient is linear between equilibrium (average $p_{eq} = 14$ mm Hg for CH_4 , 70% extraction) and the membrane over, say, one particle diameter or 0.1 cm. The relation between p_H and membrane flux (at 200 mV) reflected in Table 1 may be approximately written as

$$p_H \cong .07 (I/A) \quad (22)$$

Then equation (18), with $D_e = 0.5 \text{ cm}^2/\text{sec}$ for H_2 , becomes

$$I/A = 0.5 \left(\frac{cm^2}{sec} \right) \times \frac{14 - .07 (I/A)}{0.1} \left(\frac{mm \text{ Hg}}{cm} \right) \times 5.39 \left(\frac{amps/ft^2}{mm \text{ Hg-cm/sec}} \right)$$

and $I/A = 130 \text{ amps/ft}^2$, compared with 210 in Table 1. This calculation may be made with different sets of assumptions, but the main point is that with a realistic value of D_e , a large partial pressure gradient must exist for high H_2 flux rates. We conclude that it is plausible that diffusion may account for a substantial portion of the difference between maximum I/A as given in Table 1 and the observed values.

Flow Distribution

Nonuniform flow along both width and thickness of the cell used in this study would be very difficult to avoid. The tendency of the thin membrane to expand

irregularly presents one design problem. Flow visualization tests have shown a tendency to nonuniformity in the horizontal plane.

We have not been able to make a meaningful estimate of the effects of nonuniform flow on performance, although the cases checked have all been detrimental. For example, stagnant gas pockets in the corners would tend to become depleted of H_2 , probably inducing a potential gradient and electrolytic circuit in the plane of the membrane. This situation could occur at open circuit as well as on load, and would contribute to the observed increase of OCV with flow rate that we have previously ascribed to kinetic limitations. This problem is common to any flat rectangular gas electrode with a mixed feed; however it is accentuated with a packed gas chamber and a thin Pd-Ag anode.

Prereactor Concept

We have looked in principle at two design concepts in which the gas flows through a catalytic bed at cell temperature prior to entering the anode cell. In the case of a combination external-internal reformer, the cell is packed with catalyst. With a completely external reformer (at cell temperature), the anode chamber would not contain catalyst.

Current density would be somewhat higher in the combination reformer than in the strictly internal reformer because of better utilization of the membrane near the cell inlet. The penalty is the increased pressure drop and system volume. The best possible performance would be approximately the same as the case of the ideal catalyst and real diffusion resistance, calculated above. The second case would require very high flow rates with recycle, or series flow connection with alternating catalyst beds and anode cells. The only advantage -- flexibility in cell design -- is far outweighed by pressure drop, volume, and system complexity.

CONCLUSIONS

With a 500° F upper limit, the internal-reforming hydrocarbon anode is severely restricted by the thermodynamics of reforming. With a .001 inch activated Pd-Ag anode, 70% utilization of fuel at 1 atm total pressure, and 200 mV anode polarization, ideal performance is approximately 210 amps/ft² for methane and 190 amps/ft² for octane. Work to date has resulted in 35-45% attainment of these ideal values. Data and supporting calculations indicate that in the flow range tested, at least half of the deviation from ideal performance can be attributed to diffusion resistance between catalyst sites and membrane. Nonuniform flow distribution and kinetic limitations also contribute to the deviation although it is not possible to rank them in importance.

Higher flow velocity and a thinner bed would decrease the relative limitation due to diffusion and increase those due to catalyst and flow distribution. Changes in this direction would soon bring the cost of pumping power into significance.

Thinner and more active Pd-Ag membranes would improve performance by permitting a greater diffusion driving force between catalyst and membrane. A perfect membrane -- one with no transport resistance -- would possibly yield 20

to 30% greater current densities than obtained with the present .001 inch membranes.

If system considerations permit flow velocities high enough to have a beneficial effect on mass transport in the catalyst bed, then the design procedure should be to maximize I/A with velocity and adjust the effective length of the anode to achieve the desired utilization. This may be accomplished by using recycle, series flow connections, or baffling. A prereactor added to an internal-reforming cell would give some increase in current density at the expense of pressure drop and volume, and is best regarded as a secondary design option once the basic cell design is established.

The open-circuit voltage of a hydrogen electrode in the presence of an exponential pressure gradient is satisfactorily described by an equation that involves an average of point potentials over the anode surface. The equation gives better results than the simpler calculation where partial pressure is averaged and a single potential is determined from that average.

In summary, with a .001 inch Pd-Ag membrane at 500° F and at 1 atm total pressure, we estimate that the maximum feasible current density at 200 mV anode polarization for a liquid hydrocarbon feed with 70% utilization would be about 120 amps/ft² with a very good catalyst and careful design for gas flow.

ACKNOWLEDGMENTS

This work was part of a program sponsored by the U.S. Army Engineer Research and Development Laboratories under Contract DA-44-009-AMC-1501(T).

The author wishes to thank Messrs. J. Dafler, C. Bowman, and A. Schultz for their contributions to the work described in this paper.

NOMENCLATURE

| | |
|------------|---|
| a, L, t | cell dimensions (Figure 2) - cm |
| D | gas diffusivity - cm^2/sec |
| D_e | effective diffusivity - cm^2/sec |
| d | particle diameter - cm. |
| I/A | current density - amps/ft^2 |
| k_m | mass-transfer coefficient - cm/hr |
| k_o | limit of k_m at low flow rate (Figure 4) |
| k_r | reaction rate coefficient - hrs^{-1} |
| p_{eq} | equilibrium hydrogen partial pressure - mm Hg |
| P_H | hydrogen partial pressure - mm Hg |
| Q_F | fuel flow rate - cc/hr |
| R | gas constant |
| S_v | ideal hydrogen space velocity - hrs^{-1} |
| S_x | space velocity at mass-transfer transition (Figure 4) |
| T | temperature - $^{\circ}\text{K}$ |
| u | gas velocity - cm/sec |
| ϵ | porosity |
| η_u | fuel utilization |
| τ | tortuosity |
| F | Faraday constant |

REFERENCES

1. Gregory, D.P. and Heilbronner, H. in "Hydrocarbon Fuel Cell Technology," (B.S. Baker, ed.), p 509, Acad. Press, N.Y., 1965.
2. Hartner, A.J. and Vertes, M.A., A.I.Ch.E. - I. Chem. E. Symposium Series No. 5, 12 (1965).
3. Heilbronner, H.H., Smarz, G.A., and Kramer, S., Phase II Tech. Rept., Liquid Hydrocarbon Fuel Cell Development, Contract DA-44-009-AMC-756(T), Aug. 1965.
4. Hougen, O.A., Ind. Eng. Chem., 53, 513-515 (1961).
5. Jost, W., "Diffusion in Solids, Liquids, and Gases," pp 16-17, Acad. Press, N.Y. 1960.
6. Jurisch, E., Metz, A., and Sieverts, A., Z. anorg. u. allg. Chem., 92, 329 (1915).
7. Lieberman, B., Leeson Moos Labs., private communication.
8. Palmer, N.I., Lieberman, B., and Vertes, M.A. in "Hydrocarbon Fuel Cell Technology," (B.S. Baker, ed.), p 151, Acad. Press, N.Y. 1965.
9. Satterfield, C.N. and Sherwood, T.K., "The Role of Diffusion in Catalysis," pp 14-15, Addison-Wesley, Reading, Mass. 1963.
10. Sieverts, A. and Hagen, H., Z. phys. Chem. A174, 247 (1935).
11. Vertes, M.A. and Hartner, A.J., Fuel Cell Symp., Brussels, June 1965.

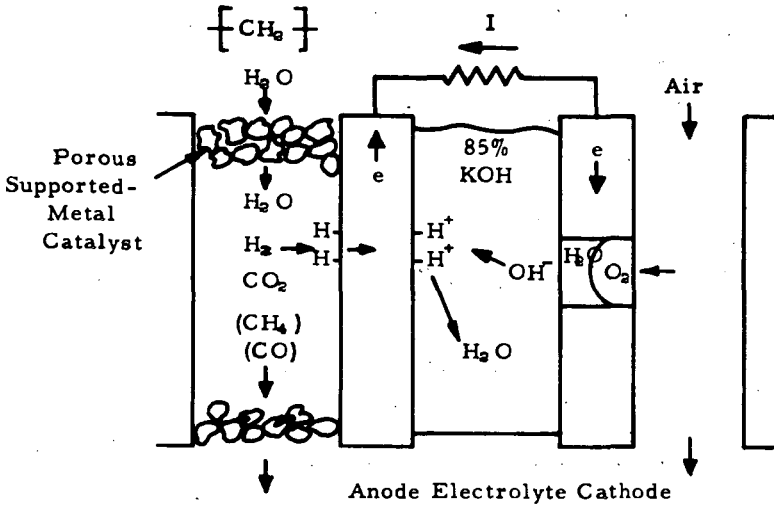


Figure 1. Operating Principle of Internal-Reforming Fuel Cell

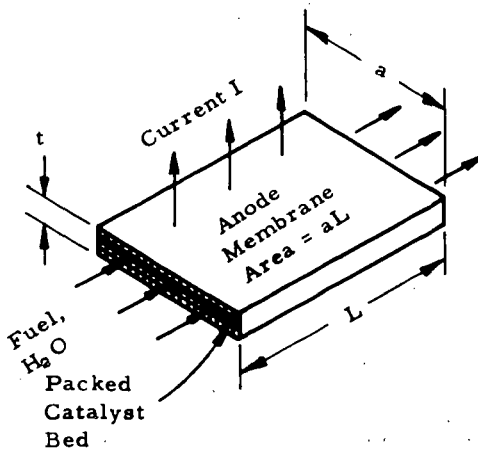


Figure 2. Anode Model Used in Analysis

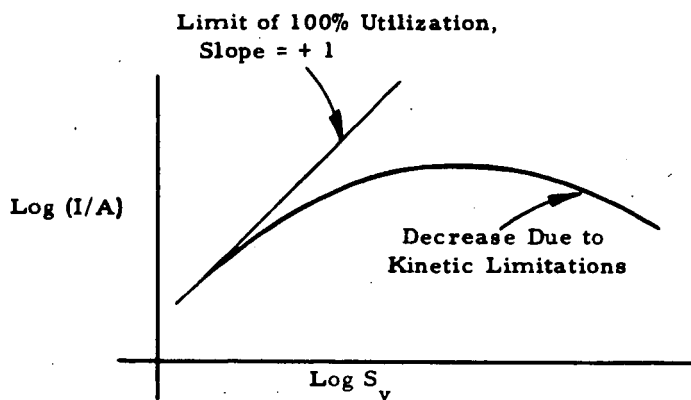


Figure 3. Dependence of Current Density on Space Velocity

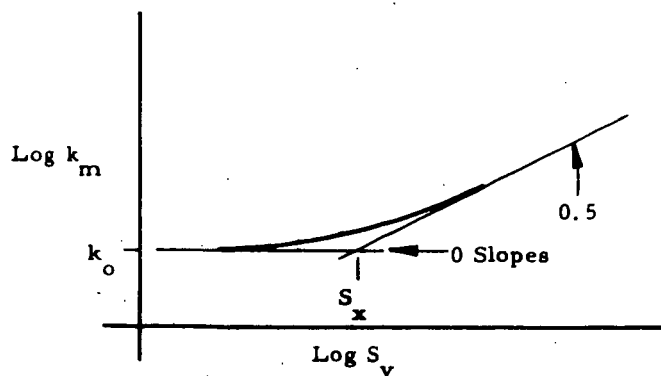


Figure 4. Dependence of Mass-Transfer Coefficient on Space Velocity in Packed Bed

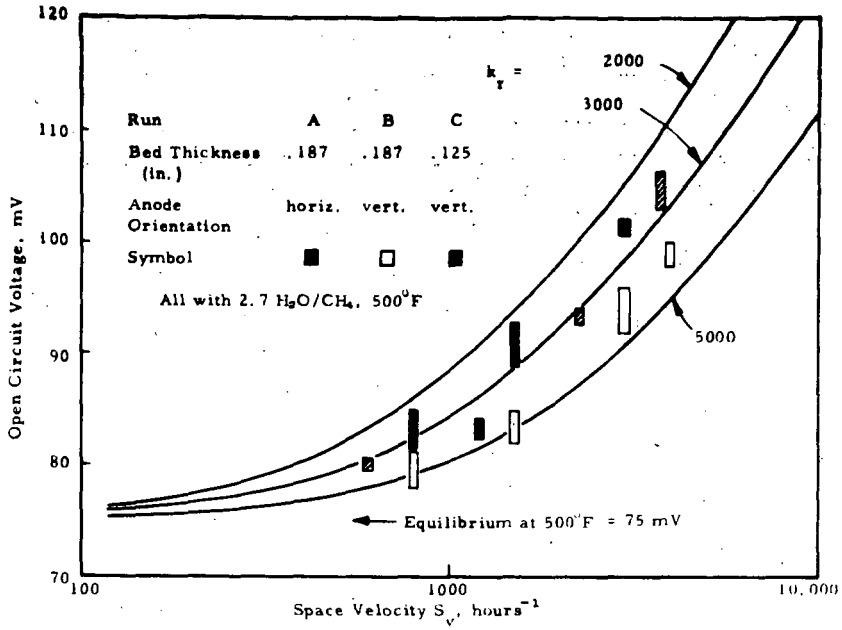


Figure 5a. OCV versus S_v - Calculated Curves by Averaging Partial Pressure (Equation 13)

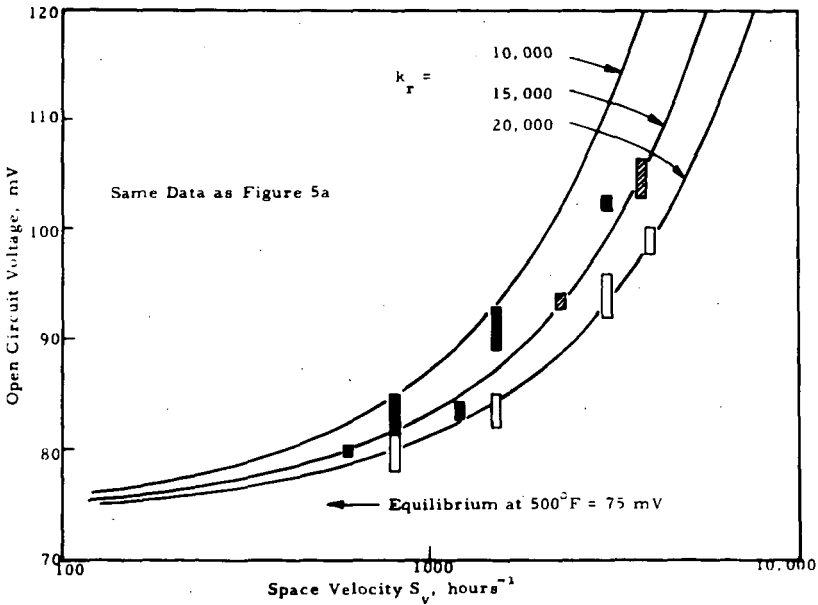


Figure 5b. OCV versus S_v - Calculated Curves by Averaging Potential (Equation 15)

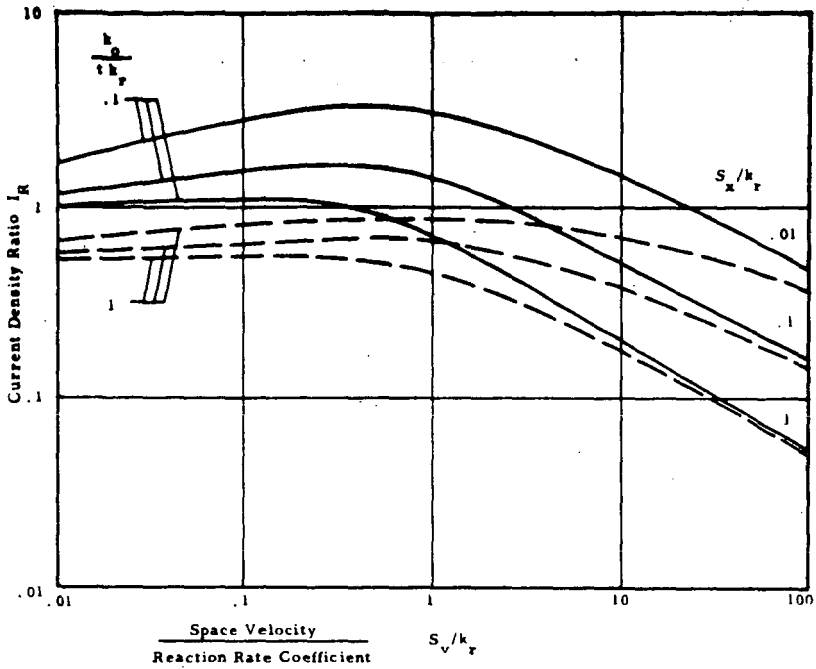


Figure 6. Dependence of Current Density on Mass Transfer and Reaction Rate Parameters (Equation 16)

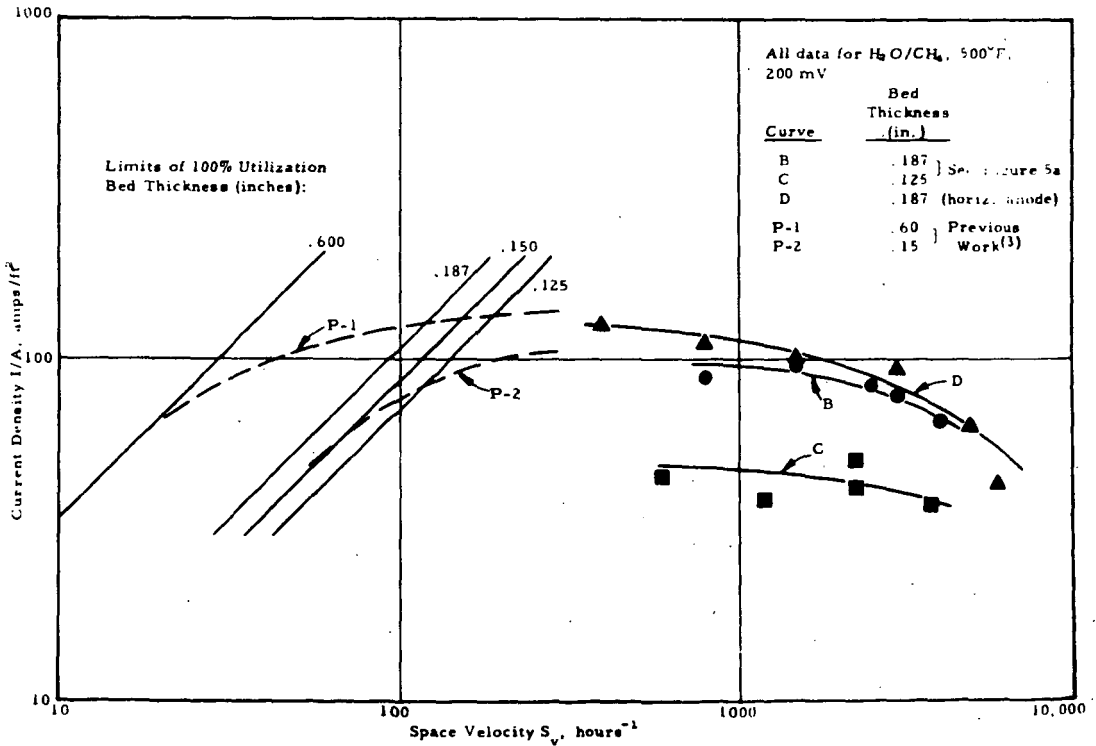


Figure 7. I/A versus S_v at 200 mV Polarization

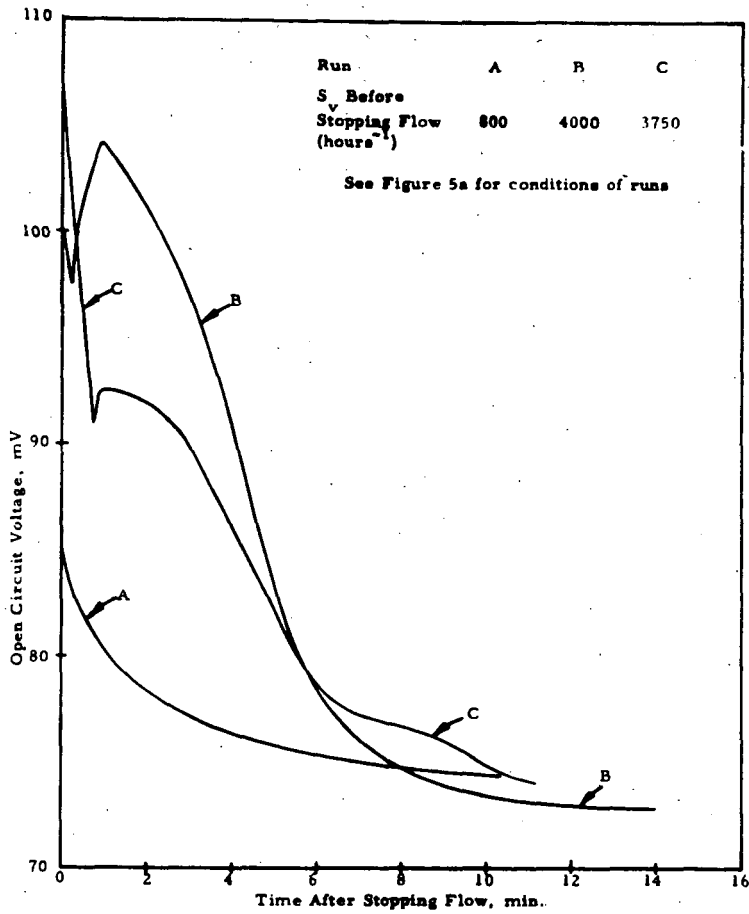


Figure 8. Transient Behavior of OCV When Flow of Fuel is Stopped